Supplementary notes on Modelling cycles and interdependence in irregularly sampled geophysical time series

Granville Tunnicliffe Wilson, John Haywood, Lynda Petherick

September 3, 2021

1 The prediction theory of stationary continuous processes

The formal theory of linear prediction for continuous time stationary series is given in Doob (1953, chap. XII sect. 5). As stated there on p. 582: *This prediction problem will be solved by reducing it to discrete parameter prediction.* Using our notation, this can be expressed in terms of the discrete sequence:

$$X_k = Z^{-k}x(t), \tag{1}$$

which can be shown, Tunnicliffe Wilson *et al.* (2015, chap. 7) to be a stationary discrete time series, with $X_k, k \leq 0$ forming a basis of the past of $x(t-h), h \geq 0$ and $X_k, k \geq 0$ forming a basis of the future of $x(t+h), h \geq 0$. The prediction of any future value $x(t+h)$ is then a linear function of the predictions of $X_k, k \geq 0$, which are linear functions of $X_k, k \leq 0$. The formal proof of the basis property is given by Doob (1953). A discrete autoregressive model of order p for X_k, in the case $k = 0$, gives, on substition of (1),

$$\varphi(Z)x(t) = \left(1 - \varphi_1 Z - \varphi_2 Z^2 - \cdots - \varphi_p Z^p\right) x(t) = n(t). \tag{2}$$

The disturbance term $n(t)$, as a consequence of being uncorrelated with $Z^k x(t)$ for $k \geq 1$, can be shown to follow a CAR(1) process with scalar coefficient κ: $dn(t) = -\kappa n(t) + dY(t)$. It is shown in Tunnicliffe Wilson *et al.* (2015, chap. 7) that (2) is a simple re-parametrization of the model (5) in the paper with the space of the coefficients φ_k being the same as that of a discrete autoregression. The innovation term $dY(t)$ is proportional to $dW(t)$ in (5). We remark that the model (5) can also be expressed as a continuous time autoregressive moving average CARMA(p, $p-1$) process with moving average operator $(\kappa + s)^{(p-1)}$, where we use the Laplace transform variable s as the differential operator. However, the numerical conditioning of this parametrization is very poor.

Historically, the methodology of continuous time prediction was developed in the setting of analogue electrical signals as described by Wiener (1949). Simple electrical circuitry was used to implement the continuous time operators. The weighting of the past associated with selected powers of Z is shown in Figure 1, reproduced from Tunnicliffe Wilson *et al.* (2015).

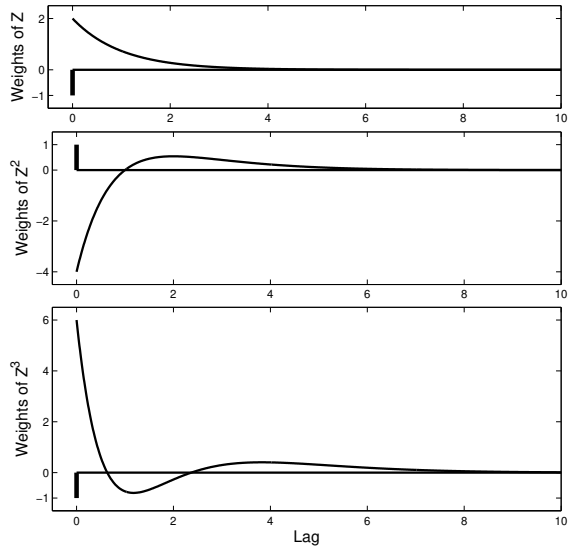

Figure 1: The weights applied to past values of the time series $x(t)$ by the continuous time generalized shift operators Z, Z^2 and Z^3. The thick line at lag zero indicates the discrete weight of -1 or +1 that is always applied at that lag by all powers of Z.

An early application of continuous time Gaussian process modelling to irregularly sampled data is found in Jones (1981) who uses a CAR(p) model. Unlike the class of discrete autoregressive models, this is not capable of approximating the second order properties of all stationary continuous processes; besides $x(t)$, the process predictors are higher derivatives of $x(t)$, which do not span the process past. A modification of this model in Belcher *et al.* (1994) does have this property and proved to be of value in practical applications. It is this model, which has been re-interpreted, extended and expounded in Tunnicliffe Wilson *et al.* (2015), that we use in the paper. The wider class of CARMA(p,q) Gaussian processes is applied to the same problem by Kelly *et al.* (2014). The models used do not involve any time scale parameter similar to the κ in our model. Otherwise, the methodology is similar, employing the Kalman filter to calculate the likelihood. The multi-modality of the likelihood is acknowledged and appropriate maximization methods employed. A range of other approaches to modelling irregularly sampled series are found in a collection of papers, Parzen (1984).

2 State space formulation of the CZAR model and its use in model fitting

Introducing $e(t)$ as the formal derivative of $W(t)$, the model (5) in the paper can be presented in continuous time state space form using the Laplace transform variable s as the differential operator, with state vector $S(t)$ having elements $S^{(k)}(t) = Z^k x(t)$ for $k = 0, \ldots, p-1$ and the innovation process $e(t)$ as the input:

$$s \begin{pmatrix} I & 0 & 0 & \cdots \\ I & I & 0 & \cdots \\ \ddots & \ddots & \ddots & \ddots \\ \cdots & 0 & I & I \end{pmatrix} \begin{pmatrix} S^{(0)}(t) \\ S^{(1)}(t) \\ \vdots \\ S^{(p-1)}(t) \end{pmatrix} =$$

$$\begin{pmatrix} \xi_1 & \xi_2 & \cdots & \xi_p \\ \kappa I & -\kappa I & 0 & \cdots \\ \ddots & \ddots & \ddots & \ddots \\ \cdots & 0 & \kappa I & -\kappa I \end{pmatrix} \begin{pmatrix} S^{(0)}(t) \\ S^{(1)}(t) \\ \vdots \\ S^{(p-1)}(t) \end{pmatrix} + \begin{pmatrix} e(t) \\ 0 \\ \vdots \\ 0 \end{pmatrix} \tag{3}$$

or $sLS(t) = RS(t) + ue(t)$, where $u = (1, 0, \ldots, 0)'$. The first row is simply the model and the remaining rows recursively generate the higher order states. The usual form of state space representation is obtained by dividing through by L, leading to the matrix differential equation

$$sS(t) = L^{-1}RS(t) + L^{-1}ue(t) = TS(t) + ve(t). \tag{4}$$

The observation equation is simply $x(t) = S^{(0)}(t)$. This representation is particularly useful for application to irregularly sampled series because the solution for $S(t)$ can be expressed conditional upon the state $S(t-r)$ at some earlier time point as

$$S(t) = \exp(Tr)S(t-r) + \int_0^r \exp(Th)\, v\, dW(t-h) = \exp(Tr)S(t-r) + w(r), \tag{5}$$

where $\exp(Tr)S(t-r)$ is the conditional expectation, or prediction, of $S(t)$ at time $t-r$ and $w(r)$ is the integrated or prediction error which is uncorrelated with $S(t-r)$, having variance

$$\mathrm{Var}\{w(r)\} = \int_0^r \exp(Th)\, v V_e v' \exp(T'h) dh. \tag{6}$$

Because of its superior numerical conditioning, we use the square root filter for state estimation. Given the estimate and its square root variance for $S(t-r)$ and the square root of $\mathrm{Var}\{w(r)\}$ computed directly from the square root of V_e, the same quantities are derived for $S(t)$. From these are derived at the successive sample times t_k the prediction errors e_k of the corresponding observations and their standard errors σ_k. The deviance quantity, minus twice

the log likelihood, is then computed as the prediction error decomposition

$$D = \sum_{k=1}^{K} \left\{ 2 \log \sigma_k + (e_k/\sigma_k)^2 \right\},$$

and minimized using an iterative algorithm. The MATLAB code used for the model estimation, and to derive the covariance and spectral properties of the fitted model, is freely available from `http://www.dependenttimeseries.com/`, together with full documentation and algorithmic descriptions. For the model including an observation noise term, the observation equation becomes $y_i = x(t_i) + \varepsilon_i = S^{(0)}(t_i) + \varepsilon_i$. Both (5) and (6) are also used for prediction and interpolation of the series and to simulate values from the model.

3 Coefficients of the models for the Dust Flux series

For the two models selected in the paper we list the estimated parameters and their t values in Tables 1 and 2. As noted in the paper, for the model with $\kappa = 0.035$ and $p = 8$ the t value of the penultimate coefficient ξ_7 is 4.28 and that of the last coefficient ξ_8 is -2.03, reflecting the prominent fall in the AIC at lag 7 and its minimum at lag 8. For the model with $\kappa = 0.01$ and $p = 20$ the t value of the final coefficient ξ_{20} is -3.47, supporting the argument for the selection of this model order. For both models the t values of the first two coefficients are large but many of the t values of the coefficients at intermediate lags are small. It would be possible to fit sub-set models with some of these coefficients removed, i.e. constrained to have values zero, as in discrete time seasonal models. Strategies for subset model selection involve further statistical testing issues, but investigation of this possibility could be worth pursuing.

k	1	2	3	4	5	6	7	8
ξ_k	0.3193	0.4502	0.0641	0.0397	0.0420	-0.1110	0.2619	-0.1264
t_k	5.9349	6.2191	0.8603	0.4729	0.5726	-1.4458	4.2758	-2.0254

Table 1: Coefficients and t values for the dust flux CZAR model with $\kappa = 0.035$ and $p = 8$

k	1	2	3	4	5	6	7	8	9	10
ξ_k	0.3843	0.5344	-0.1169	0.1344	-0.0613	-0.0466	-0.0438	0.0143	0.0663	0.0479
t_k	6.2478	8.6149	-1.3332	1.6141	-0.7229	-0.5483	-0.5050	0.1677	0.8006	0.5372
k	11	12	13	14	15	16	17	18	19	20
ξ_k	-0.1540	0.0692	0.0611	-0.0395	0.0670	-0.0082	-0.0292	0.0320	0.0753	-0.2282
t_k	-1.8850	0.8134	0.7221	-0.4445	0.7695	-0.0943	-0.3301	0.3711	1.1156	-3.4733

Table 2: Coefficients and t values for the dust flux CZAR model with $\kappa = 0.01$ and $p = 20$

4 The model faithfully represents the series structure

We are not aware of any independent methodology for fully confirming the effectiveness of our modelling procedure for faithfully representing the structure of an irregularly observed stationary process. In the following section of this supplementary document, we show that the Lomb-Scargle approach is not sufficiently reliable in this respect. However, we present here two exercises that provide support for our procedure in the context of the dust flux example. The first is to use binning of the data into the form of a discrete time series, from which a conventional spectral estimate can be formed over lower frequencies. Over this limited range of frequencies our model spectrum is consistent with this conventional spectrum. The second exercise is to construct a simulation of a sample series from our fitted model at equal time intervals of 4 years. From this, a conventional spectral estimate can again be formed, but over a wider frequency range. As expected, this is consistent with our model spectrum, but serves to validate the simulation. A further simulation of a sample series from the same fitted model, but at the same time points as the original data, is then constructed. On fitting the same model with order $p = 20$ and $\kappa = 0.010$ we find that its spectrum faithfully reproduces the spectrum of the simulating model.

The results are displayed in Figure 2. The plot on the left is of the spectrum of the discrete series formed from the flux data by binning and averaging it in 100 equally spaced intervals. It is shown on the same scale as the plots in Figure 6 in the paper, but necessarily truncated at the Nyquist frequency corresponding to a period of 800 yrs. The value of this plot is in its

confirmation of the two low frequency peaks seen in the right hand plot of Figure 6. Binning does not particularly distort the low frequency components of the series, and gives support to the presence of a broad low frequency spectral peak.

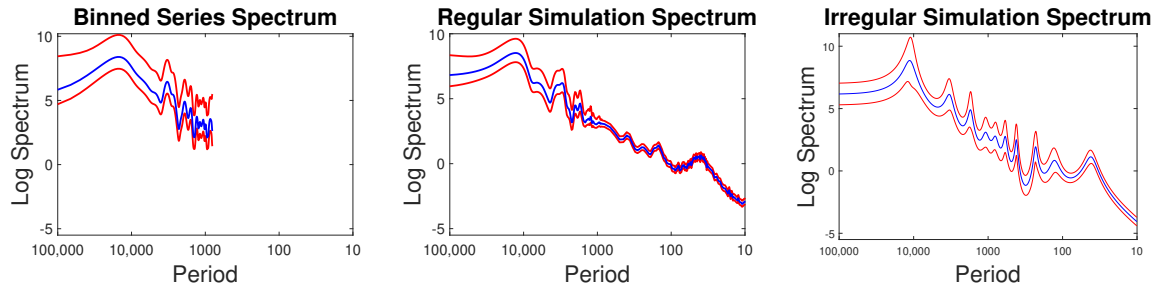

Figure 2: On the left the smoothed spectrum of the logarithms of the flux series obtained by binning the series into 100 intervals. In the centre the smoothed spectrum of the series in Figure 3 sampled at regular intervals of 4 years. On the right the spectrum of the CZAR model of a simulation from the fitted model for the dust flux series.

The plot in the centre of Figure 2 is the spectrum of the regularly spaced simulated series, which spans 100,000 years. This simulated series is shown in Figure 3 after reversing the logarithmic transformation and sub-sampling at intervals of 60 years, which provides more similarity in appearance with the original series. The spectrum, by its similarity to the model spectrum on the right of Figure 6, validates the simulation as arising from that model spectrum. With that validation, the plot on the right of Figure 2 confirms that our estimation procedure efficiently recovers the spectral structure from a simulated sample of that model at the irregular time points.

5 Direct spectrum estimates for the Dust Flux series

In the paper we cite the Lomb-Scargle method, Lomb (1976), Scargle (1982, 1989) as a means of directly estimating the spectrum of irregularly sampled time series. This is widely applied in the field of astronomy for identifying periodicities in light curves of astronomical

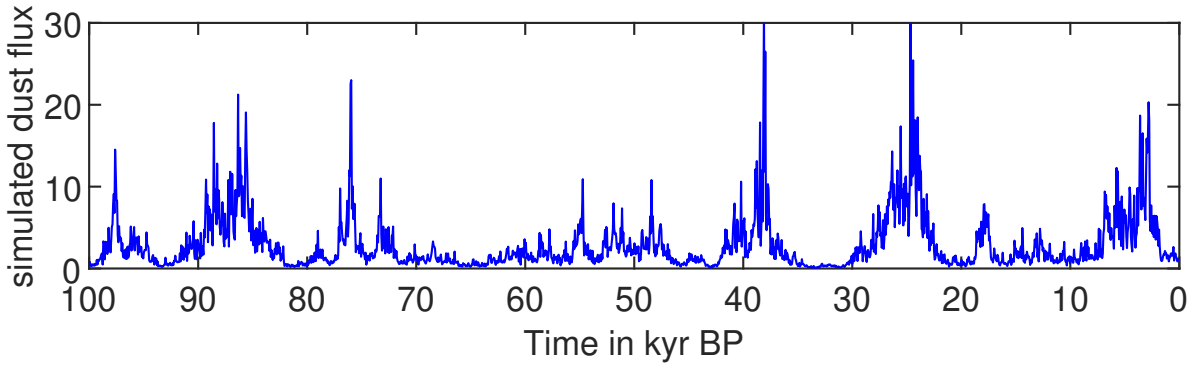

Figure 3: A plot of a simulation from the flux model with $\kappa = 0.010$ and $p = 20$ at intervals of 60 years.

objects, which are unavoidably measured intermittently due to varying observational conditions. Similar methodology appears earlier in Vaníĉek (1969, 1971) and is also known as the Gauss-Vaníĉek or G-V method. An in-depth analysis of the method is presented by VanderPlas (2018). The method is not computationally demanding, with ample publicly available software implementations. These simply fit the cosine-sine pair of cycles separately to the available data points at each of a grid of frequencies. The spectrum is measured by the variance accounted for. The user specifies an upper limit for the frequency grid, set as a multiple of the Nyquist frequency derived as if the observations were equally spaced. The significance of the spectrum at any point is determined on the null hypothesis that the series is a sample from white noise. For our series this is clearly not valid, so we will not attempt to construct any indicators of significance or sampling limits on the smoothed spectrum.

We now present results of direct spectral analysis of the dust flux series using this method for comparison with the results of our CZAR process modelling. It will be seen that they are substantially different. We conclude that the Lomb-Scargle method has serious limitations when applied to this series.

The first plot on the left of Figure 4 shows the Lomb-Scargle spectrum with the smoothed spectrum superimposed, though we cannot sensibly determine error limits on this. The smooth-

ing transitions from a low bandwidth at low frequencies to a higher one at high frequencies so as better to reveal the features on the logarithmic frequency scale. We compare this spectrum with that shown for our model on the right of Figure 6 in the paper. At lower frequencies some similarity is to be seen with the peaks at periods of 14000 years and 3000 years. The smoothed spectrum then falls away until around the period of 1000 years before rising steadily to higher frequencies. Small peaks are seen close in frequency to the high frequency peak of our model spectrum.

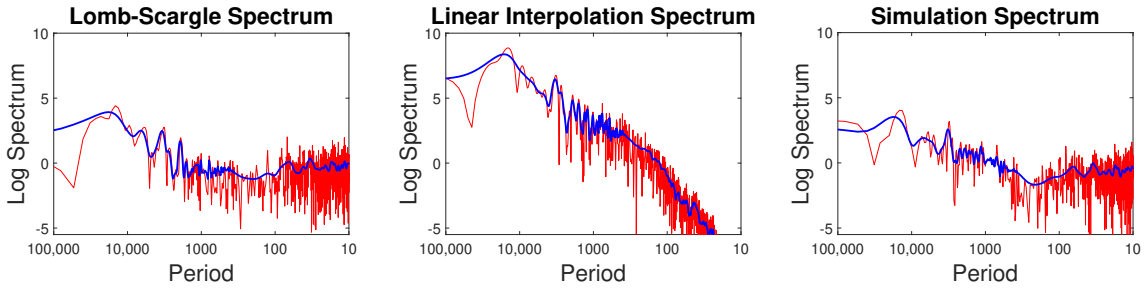

Figure 4: Plots of spectra of the logarithms of the flux series obtained, on the left using the Lomb-Scargle method, in the centre from linear interpolation of the series. On the right the Lomb-Scargle of a simulation from the CZAR model.

Having, by the exercise presented in the previous section, confirmed that our model does faithfully estimate the series spectrum, we look for understanding of why the general shape of the Lomb-Scargle spectrum estimate is so different. This may be found in Cornette (2007) who points out that the G-V spectrum (as he calls the Lomb-Scargle) is very close to that of the Fourier Transform power spectrum (FTPS). Calculation of the FTPS requires the series time points to be rounded to a fine discrete grid, and unknown values at other grid points replaced by zeros. This is conveniently achieved for the flux series because the times are given to the nearest 0.5 year, and gives some insight into the reason for the limitations of this approach. Using zero for unknown values is equivalent to interpolating the series on the assumption that it is uncorrelated white noise. That assumption imposes a prior form of a uniform (constant)

spectrum, which explains the relatively level spectrum that is seen in the left hand plot of Figure 4. An alternative is linear interpolation of the series which is equivalent to assuming that it is a realization of a random walk. The central plot of Figure 4 shows the spectrum after applying linear interpolation at the same grid points. This prior form gives a smoothed spectrum more similar to that of our model, though falling away more rapidly. A small peak is also seen at the same frequency, with period 42, as the more prominent high frequency peak in our model spectrum. The plot on the right of Figure 4 is of the Lomb-Scargle spectrum of a simulation of our CZAR model at the same sampling points as the original series. It is similar to the plot for the original series spectrum on the left. The Lomb-Scargle method does not give a fair picture of this model spectrum.

6 Using the variogram to identify an observation noise term

The sample variogram is a widely used tool for characterizing the dependence between measurements made at irregularly scattered points in one or more dimensions. For a stationary process $X(t)$ in one dimension the theoretical (semi-)variogram is defined at lag h as $\gamma(h) = \mathrm{Var}[X(t+h) - X(t)]/2$. It is related to the covariance function of the process by $\gamma(h) = \mathrm{Var}\,X(t) - \mathrm{Cov}[X(t+h), X(t)]$, but has the advantage that it is also well defined for an integrated process such as a random walk. For an irregularly sampled series $x_i = x(t_i)$ it may be estimated at lag h by averaging the squared differences $x_i - x_j$ for all pairs of points separated by a lag $t_i - t_j$ within some set tolerance of h, known as a bin. The wider the tolerance the lower the variance of the estimate, but the less the resolution of the variogram form. To illustrate the value, and limitations, of the (sample) variogram for identifying an observation noise term, we show in Figure 5 the estimated autocorrelation of the final CZAR model, including an observation noise term, fitted to the temperature series. In the centre we show the sample variogram of the same series. The model ACF shows 2 standard error limits and though the cyclical

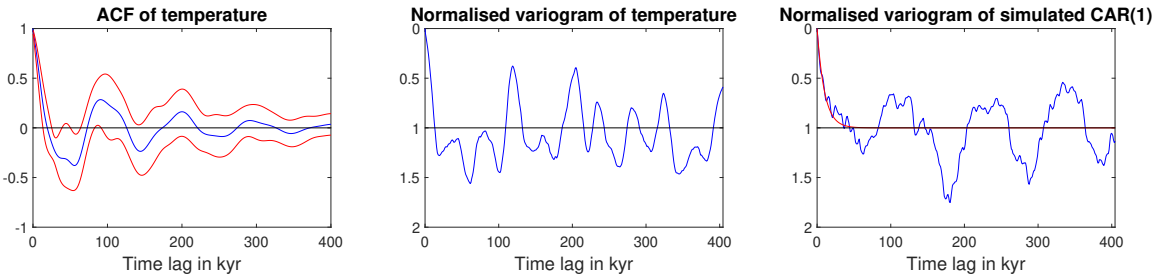

Figure 5: On the left the estimated autocorrelation function of the final CZAR model, including an observation noise term, fitted to the temperature series. In the centre, the variogram of the same series, scaled and inverted for comparability with the autocorrelations. On the right, the theoretical variogram of a CAR(1) process (red) and the sample variogram of a realisation from the process at the same time points as the temperature series. The bin width for the variograms is approximately 2kyr and the maximum lag is 400kyr.

pattern is evident, associated with an irregular cycle of approximately 100kyr, the limits are quite wide. Given that the number of points in the series is well over 5000 we might expect the error limits on the variogram to be much narrower. However, for a highly correlated series the number of effectively uncorrelated points can be much smaller, resulting in high standard errors. These are also difficult to compute without knowledge of the underlying process. This point is illustrated by the plot on the right of Figure 5. This shows the theoretical variogram of a CAR(1) process and the sample variogram of a realisation from the process at the same time points as the temperature series. The magnitude of the sampling variation is considerable, with the values beyond lag 100 kyr having a spurious irregular cyclical appearance.

However, the main point of this section is how we might gain some indication of the presence and magnitude of observation noise from the variogram. In the plot on the left of Figure 5 this noise term is evidenced by the immediate but barely visible fall of the acf from 1.0 at lag 0 to 0.97 at the next plotted point at 0.04kyr. There is also a slight indication of a similar appearance in the variogram in the centre of Figure 5. However, for this data set neither of these

effects is clear and definite on the scale shown, because the noise term variance is only 0.03 of the series variance. This is not, however, negligible; the standard deviation of the noise term is 0.17 that of the series which cannot be ignored, and including observation noise terms in the CZAR model improves its parametric efficiency and its representation of the spectral properties. The initial CZAR model without inclusion of the observation noise terms was valuable in revealing the need for these terms as illustrated by Figure 10 in the paper.

7 Causality and observation noise

We present here simple examples of discrete autoregressive models to illustrate aspects of Granger causality relevant to our models.

7.1 Two-directional causality

The first example is of a pair of series y_t and x_t generated from a first order bivariate autoregression with disturbances e_t and f_t which we take to be independent white noise series. Granger causality can, though, allow contemporaneous correlation in these, because evidence of causality is taken to be the predictive value of strictly past values. We assume that the model is stationary and that all coefficients a, b, c, d are non-zero.

$$y_t = ay_{t-1} + cx_{t-1} + e_t \tag{7}$$

$$x_t = dy_{t-1} + bx_{t-1} + f_t. \tag{8}$$

In this case both series are said to be causal for the other. For example, because y_{t-1} and x_{t-1} are not collinear, the regression in the first line, with error e_t uncorrelated with the predicting variables, will necessarily result in an increased residual variance if x_{t-1} is removed from that regression. Therefore we say that x is (Granger) causal for y.

If, however, the coefficient c has the value zero, we would say that x is not causal for y. Removing x_{t-1} from this regression when $c = 0$ would not increase the residual variance.

7.2 Apparent causality due to a third variable

The second example concerns the requirement that causality be tested in the wider context of any other, related, series. Thus an apparent causal relationship between two series may be explained by a third series, and is no longer evident when that series is introduced. This is quite intuitive if the effect of the third series is delayed more on one series than the other. For this example we need a trivariate model which we again assume is stationary with non-zero coefficients and completely independent disturbances:

$$y_t = ay_{t-1} + cz_{t-2} + e_t \tag{9}$$

$$x_t = dz_{t-1} + bx_{t-1} + f_t \tag{10}$$

$$z_t = rz_{t-1} + g_t. \tag{11}$$

As written, neither x nor y is causal for the other; z is causal for both. The argument in this case is best illustrated graphically. We set $a = 0.8$, $b = 0.7$, $c = 2$, $d = 1$, $r = 0.9$, $\mathrm{Var}\, e_t = 2.5$, $\mathrm{Var}\, f_t = 1.5$ and $\mathrm{Var}\, g_t = 0.5$. Figure 6 shows that when z_t is not used as a predicting variable, there is evidence for Granger causality of y by x, because including past values of x reduced the prediction error variance. For our Antarctic ice core series we have included in the paper mention of the theory that solar insolation is causal for the glacial-interglacial cycles reflected in our series. This does not necessarily invalidate our evidence for the causal dependence of each of our two series on the other, especially if the effect of insolation is directly on the temperature series alone, and not on the carbon dioxide, as might be expected from the physical science. On setting $d = 0$ in the above model the evidence for the causal effect of x_t on y_t vanishes.

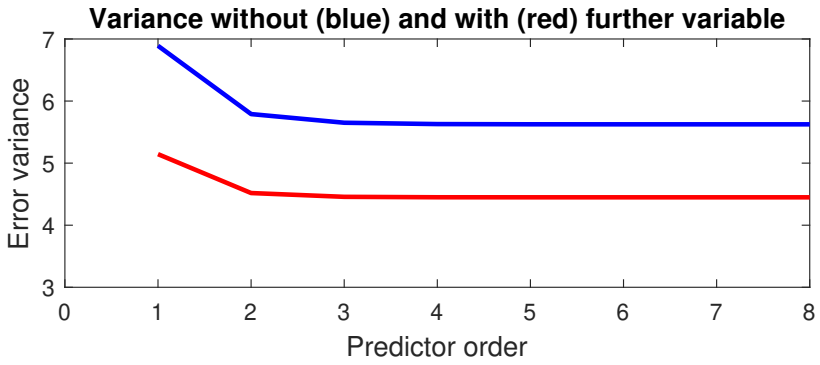

Figure 6: In blue, the prediction error variance of the series y_t plotted for increasing order of autoregression on its own past alone. In red, the variance when the autoregression also includes past values of x_t.

7.3 Apparent causality due to observation noise

The third example is that of added noise on the series x_t in the context of just the two series with y_t alone being dependent on x_t. The model is therefore

$$y_t = ay_{t-1} + cx_{t-1} + e_t \tag{12}$$

$$x_t = bx_{t-1} + f_t. \tag{13}$$

Consider now that x_t is not observed directly, but only with added noise as $X_t = x_t + h_t$, where the uncorrelated series h_t is independent of both e_t and f_t. As the pair of equations stand, y_t is not causal for x_t, but it does become Granger causal for X_t. Intuitively, past values of y_t contain

some information about x_t which is obscured in X_t, and this helps to predict X_t. Figure 7 shows in blue the prediction error variance of X_t from its own past, and in red that when past values of y_t are also included.

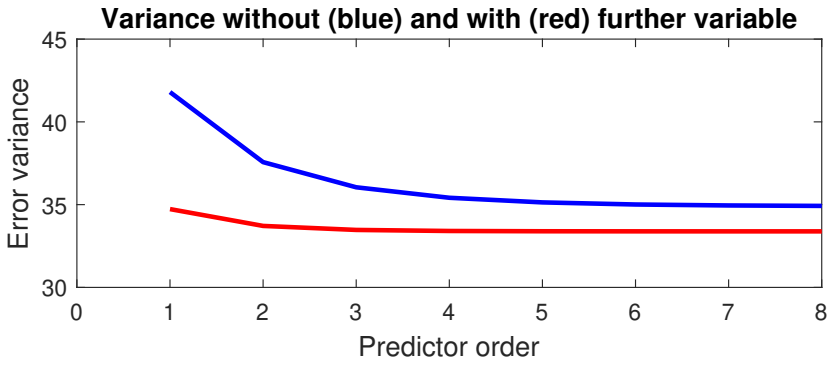

Figure 7: In blue, the prediction error variance of the series X_t plotted for increasing order of autoregression on its own past alone. In red, the variance when the autoregression also includes past values of y_t.

Although the variance reduction is not so marked in this example, the proper inclusion of an observation noise term in the model can eliminate this possible source of misinterpretation of causality.

8 Model simulation of the Antarctic ice core series

The figure below shows, in the first line, the true Antarctic ice core measurements of atmospheric carbon dioxide concentration and temperature. In the line below are shown simulations

of these series generated at the same observation time points from the first bivariate CZAR model fitted to the series with $\kappa = 0.0008$ and $p = 14$. This model therefore incorporates the features of low lag autocorrelation, shown in Figure 10 of the paper, which are represented in the explicit observation noise terms of the final model of lower order. This is an independent realization of a Gaussian process model and can only conform in its statistical summaries and not its actual values. But it does expose the model to criticism if its general appearance is, on visual evidence, very different from that of the modelled series. It appears in this case that the simulation has a very similar appearance to the true series. Similar comment applies to the simulation of the dust flux series shown in Figure 3 above.

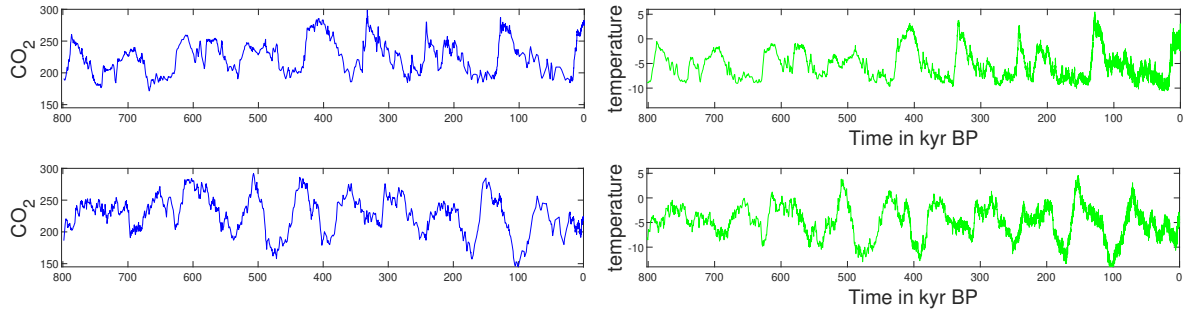

Figure 8: Above, the Antarctic ice core measurements of atmospheric carbon dioxide concentration ppmv and temperature °C. Below, simulations from the model fitted to this data, at the same sampling times.

References

Belcher, J., Hampton, J. S., & Tunnicliffe Wilson, G. 1994. Parameterisation of continuous time autoregressive models for irregularly sampled time series data. *Journal of the Royal Statistical Society: Series B*, **56**, 141–155.

Cornette, J. L. 2007. Gauss-Vaníček and Fourier transform spectral analyses of marine diversity. *Computing in Science and Engineering*, **9**(4), 61–63.

Doob, J. L. 1953. *Stochastic Processes*. New York: Wiley.

Jones, R. H. 1981. Fitting a continuous time autoregression to discrete data. *Pages 651–682 of:* Findley, D. F. (ed), *Applied Time Series Analysis III*. New York: Academic Press.

Kelly, B. C., Becker, A. C., Sobolewska, M., Siemiginowska, A., & Uttley, P. 2014. Flexible and scalable methods for quantifying stochastic variability in the era of massive time-domain astronomical data sets. *The Astrophysical Journal*, **788**, 33.

Lomb, N. R. 1976. Least-squares frequency analysis of unequally spaced data. *Astrophysics and Space Science*, **39**, 447–462.

Parzen, E. A. 1984. *Time Series Analysis of Irregularly Observed Data*. New York: Springer-Verlag.

Scargle, J. D. 1982. Studies in astronomical times series analysis II: statistical aspects of spectral analysis of unevenly spaced data. *The Astrophysical Journal*, **263**, 835–853.

Scargle, J. D. 1989. Studies in astronomical time series analysis III: Fourier transforms, auto-correlation functions, and cross-correlation functions of unevenly spaced data. *The Astrophysical Journal*, **343**, 874–887.

Tunnicliffe Wilson, G., Reale, M., & Haywood, J. 2015. *Models for Dependent Time Series*. New York, CRC Press.

VanderPlas, J. T. 2018. Understanding the Lomb–Scargle periodogram. *The Astrophysical Journal Supplement Series*, **236**(1), 16.

Vaníĉek, P. 1969. Approximate spectral analysis by least-squares fit. *Astrophysics and Space Science*, **4**, 387–391.

Vaníĉek, P. 1971. Further development and properties of the spectral analysis by least-squares fit. *Astrophysics and Space Science*, **12**, 10–33.

Wiener, N. 1949. *Extrapolation, Interpolation and Smoothing of Stationary Time Series.* New York: Cambridge.